🔓**Open Access**

All-Fiber Saturable Absorbers for Ultrafast Fiber Lasers

(Invited Paper)

Wei Zhao
Guangwei Chen
Wenlei Li
Guomei Wang
Chao Zeng
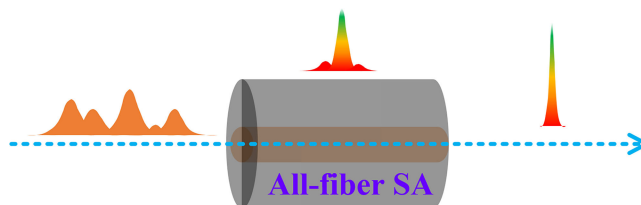
All-fiber SA

IEEE

All-Fiber Saturable Absorbers for Ultrafast Fiber Lasers

(Invited Paper)

Wei Zhao,[1,2] **Guangwei Chen** [1,2,3] **Wenlei Li,**[1,2,4]
Guomei Wang [1,2,5] **and Chao Zeng** [1,2]

[1]State Key Laboratory of Transient Optics and Photonics, Xi'an Institute of Optics and Precision Mechanics, Chinese Academy of Sciences, Xi'an 710119, China
[2]University of Chinese Academy of Sciences (UCAS), Beijing 100049, China
[3]Beijing Laboratory of Optical Fiber Sensing and System, Beijing Information Science & Technology University, Beijing 100016, China
[4]School of Physics and Electronic Information, Henan Polytechnic University, Jiaozuo 45400, China
[5]School of Physics and Optoelectronic Engineering, Shandong University of Technology, Zibo 255049, China

Abstract: The past decade has witnessed tremendous achievements of ultrafast fiber laser technologies due to rapid developments of saturable absorbers (SAs) based on, in particular, nanomaterials such as 0D quantum dot, 1D carbon nanotubes, 2D layered materials, and 3D nanostructures. However, most of those nanomaterials-based SAs are inevitably absence of the high damage threshold and all-fiber integration, therefore challenging their applications on highly integrated and high-energy pulse generations. Recently, the real all-fiber SAs based on the nonlinear multimodal interference (NLMMI) technique using multimode fibers are demonstrated to overcome the above limitations. In this review, a detailed summary of the recent advances in NLMMI-based all-fiber SAs is provided, including the fundamental theory, implementation scenarios, and ultrafast fiber lasers of the all-fiber SAs, covering wide wavelength range of 1, 1.55, and 2 μm. In addition to the state-of-the-art overview, optical rogue waves in the all-fiber SA-based ultrafast fiber laser are extensively analyzed, which reveals the laser physics behind the dynamics from low-energy to high-energy pulses and directs the design of high-energy ultrafast fiber lasers. The conclusions and perspectives of the all-fiber SAs are also discussed at the end.

Index Terms: Ultrafast fiber laser, saturable absorber, nonlinear multimode interference effect, high-energy pulse generation, optical rogue wave.

1. Introduction

Ultrafast lasers with ultrashort pulse duration and broad spectral tuning capability have been the focus of attention across many physical settings, such as plasmas, condensed matter, nonlinear optics and telecommunication systems [1]–[5]. Mode-locked fiber lasers are powerful sources for generating ultrafast pulses. As a solitary wave solution of localized nonlinear wave, temporal
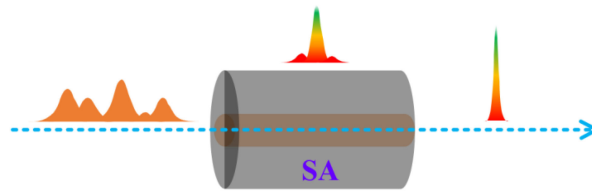
Fig. 1. Schematic of self-amplitude modulation of SAs.

solitons generated in mode-locked fiber lasers have widespread applications in biology, telecommunication, spectroscopy and scientific research [6]–[10]. The lossy elements in mode-locked fiber laser, saturable absorbers (SAs) occupy a critical position in self-starting and maintaining stable mode–locking by mode beating effect [11], [12]. The self-amplitude modulation of light in the lasers, resulting from SAs, can discriminate against the low-intensity parts of pulse and bring minimal influence to bear on high-intensity ones, as shown in Fig. 1 [9], [13].

The original SA for generating ultrafast pulses is real material, displaying intrinsic nonlinear decrease of absorption with increasing incident light intensity [1], [13]. A dominate technique for achieving passively mode–locking operation is semiconductor saturable absorber mirrors (SESAMs), which are based on resonant nonlinearities involving carrier transitions in semiconductor materials. The saturable absorption of SESAMS results from bandfilling process termed as Pauli blocking or phase space filling [14]–[16]. The transfer function of SESAMs can be approximated as [9], [12]

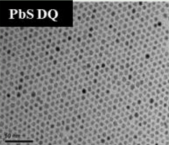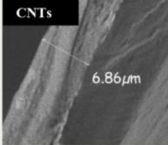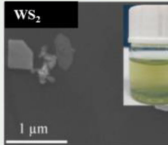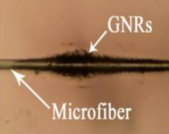$$\alpha = \frac{\Delta\alpha}{1 + I/I_{sat}} + \alpha_{ns},$$ (1)
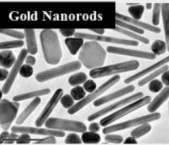
where $\Delta\alpha$, α_{ns}, I and I_{sat} denote modulation depth, unsaturable absorption, transient intensity and saturable intensity of pulse, respectively. Because of mature semiconductor technique, response time of nonlinearity in SESAMs can be flexibly tuned from femtoseconds to nanoseconds [17], [18]. The carriers' dynamic processes of intraband thermalization and interband recombination in SESAMs present two instinct time scales, governing the progression of mode–locking. In mode–locked fiber lasers, SESAMs are incorporated into cavities by mounted on a single mode fiber with connector and solitons have been achieved [19]–[21]. However, SESAMs' operating bandwidth is limited by bottom distributed Bragg reflectors, and their fabrication faces severe challenge in the range of 1.3–1.5 μm [15], [22].

Carbon nanotubes (CNTs) discovered in the year of 1993 provides a promising solution for achieving flexible and wideband mode-locked fiber lasers [23]. CNTs are direct–bandgap 1D nanomaterials, whose nonlinear absorption root in resonant effect and rely on the distribution of their tube diameters [15], [24]–[26]. Since successfully applied to mode–locked fiber laser by Set's group in 2003 [27], CNTs have been at the center of scientific research on mode–locking, for the advantages of large optical nonlinearity, broad operation bandwidth and ultrafast recovery time [28]–[30]. Next year, monolayer graphene is isolated from graphitic by Novoselov and Geim [31]. Until 2009, the atomic–layer graphene exhibiting saturable absorption was demonstrated in mode–locked fiber lasers [32]. The remarkable progress of graphene in mode–locking displays a spillover effect, arousing great research interest in low–dimensional nanomaterials [33]–[44], as shown in Table 1. Studies have shown that 0D quantum dot displays outstanding nonlinear saturable absorption properties, for example PbS quantum dot with modulation depth up to 44.5% [35]. Zhang *et al.* reported that 2D layered–material such as black phosphorus and TiS$_2$, a typical transition metal dichalcogenides could be acted as wide-range adjustable SAs for mode–locking [36], [38]. Mao *et al.* demonstrated that 3D Fe$_2$O$_3$ nanoparticles exhibit broadband saturable absorption, which have been applied for near-infrared fiber lasers and cylindrical vector lasers [40]. However, the low damage threshold of most nanomaterials–based SAs confines the applications of high-energy pulses generations.

Fiber laser possesses fascinate features of compactness, and high reliability resulting from the all–fiber construct, which will be broken by insertion of materials–based SA. Nonlinear amplify-

TABLE 1

Nanomaterials-Based SAs Including 0D Quantum Dot [35] (Figure reproduced with permission from [35] © 2018 Photonics Research), 1D CNTs [42] (Reproduced from [D.Mao, T. Feng, W. Zhang, H. Lu, Y. Jiang, P. Li, B. Jiang, Z. Sun, and J. Zhao, "Ultrafast all-fiber based cylindrical-vector beam laser," Appl. Phys. Lett., vol. 110, no. 2, Jan. 2017, Art. no. 021107], with the permission of AIP Publishing), 2D layered materials [37] [Reprinted/Adapted] with permission from [ref 37], and 3D nanostructures [41] (Reproduced from [X. D. Wang, Z. C. Luo, H. Liu, M. Liu, A.-P. Luo, and W.-C. Xu, "Microfiber-based gold nanorods as saturable absorber for femtosecond pulse generation in a fiber laser," Appl. Phys. Let., vol. 105, no. 16, Oct. 2014, Art. no. 161107], with the permission of AIP Publishing)

ing loop mirrors (NALMs) and nonlinear polarization rotation (NPR) technique, whose saturable absorption is based on nonlinear effect or nonlinear switching technique, provide feasible solutions to avoid this problem. Unfortunately, the intensity-dependent transmissions of NPR- and NALMs-based modulators increase with a non-monotonous behavior and should operate close to stability threshold, which will lead to pulse destabilization and multi-pulsing. Additionally, a precise control of power splitting and expense of efficiency and output power are required to the acquisition of self-starting and saturation effect of NALMs [4], [28], [45]–[50]. As a member of nonlinear switching technique, nonlinear multimodal interference (NLMMI) effect based on multimode fiber shows the similar intensity–dependent transmission, and has been demonstrated to be a SA [51]–[53]. The NLMMI–based all–fiber SAs consist of multimode fiber and single mode fiber (SMF), which possess intriguing properties as diverse as easy to integrate, low–cost, versatility, high damage threshold and an instantaneous response time. Since predicted theoretically by Nazemosadat and Mafi in 2013, the all–fiber SAs have attracted enormous interest of researchers for acquiring ultrafast pulse in fiber lasers [54]–[58]. Given that the controllable spatiotemporal nonlinear effects and relative small nonlinear coefficient in multimode fiber, the all–fiber SAs could operate at a much higher power level than NPR and most material based SA, which provides a potential solution for highly-integrated and high-energy pulse generations [51], [58]–[60]. Moreover, numerous novel nonlinear phenomena will give a new insight into ultrafast fiber lasers and mirror laser physics, attributing to the complex nonlinearity and dispersion in a piece of multimode fiber.

In this Review, the popular techniques for ultrafast pulse generation in fiber lasers and emerging researches of the all–fiber SAs for mode–locking are summarized. In Section 2, the fundamental theories of NLMMI–based SAs with saturable absorption, spectral filtering effect and implementation scenarios for mode–locking are presented. In Section 3, the recent advances of all–fiber SAs in ultrafast fiber lasers including erbium–, ytterbium–, and thulium–doped fiber lasers are provided. In Section 4, optical rogue wave for generating high–energy pulses in all-fiber SA-based fiber lasers
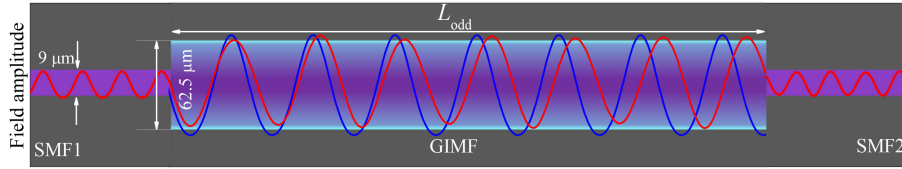
Fig. 2. The schematic structure of SMF–GIMF–SMF. Blue and red lines denote lights under low and high power cases, respectively [58]. Figure reproduced with permission from [58] © Photonics Research.

are detailed analyzed. In the last section, the emerging trends, opportunities and challenges for all–fiber SAs applied in ultrafast fiber lasers are discussed.

2. Basic Characteristics and Implementation of All–Fiber SAs

In this section, the fundamental theories containing saturable absorption and spectral filtering, and implementation scenarios of NLMMI–based all–fiber SAs are presented. The typical multimode fibers having been used in the SAs include graded-index multimode fiber (GIMF) and step-index multimode fiber (SIMF). Here, GIMF is chosen as an example to discuss in this section. A schematic structure of all–fiber SAs is shown in Fig. 2 [58].

2.1 NLMMI Effect and Saturable Absorption

When light is launched into GIMF, fundamental mode in SMF1, $E_0(\rho, \phi, 0)$ excites the p-order guided mode of GIMF $F_p(\rho, \phi, 0)$ with slow varying amplitude envelop A_p [54],

$$E_0(\rho, \phi, 0) = \sum_p F_p(\rho, \phi, 0) A_p. \tag{2}$$

The mode fields evolve into $E(\rho, \phi, z)$ after propagating z distance along GIMF,

$$E(\rho, \phi, z) = \sum_p F_p(\rho, \phi, 0) e^{j\beta_p z} A_p = e^{j\beta_1 z} \sum_p F_p(\rho, \phi, 0) e^{j(\beta_p - \beta_1)z} A_p, \tag{3}$$

where β_1, β_p denote the 1- and p-order propagation constant, respectively, which are frequency–dependent and can be expanded using Taylor series at fundamental frequency ω_0 of modes. In linear case, because of their diverse group velocities, the modes excited in GIMF separate and oscillate in a periodic interference pattern with a period of $Z = \pi R / \sqrt{2\Delta}$ owing to MMI effect, where R and Δ denote the radius and index difference between the center and the cladding of GIMF, respectively. In the weak coupling regime and nonlinear case, evolution of A_p can be expressed by Manakov equation [60]–[62]:

$$\frac{\partial A_p}{\partial z} - i\delta\beta_p^{(0)} A_p + \delta\beta_p^{(1)} \frac{\partial A_p}{\partial t} + i\frac{\beta_p^{(2)}}{2} \frac{\partial A_p^2}{\partial t^2} = \frac{in_2\omega_0}{c} \left(\frac{8}{9} f_{pppp} |A_p|^2 + \frac{4}{3} \sum_{i \neq p} f_{ppii} |A_i|^2 \right) A_p. \tag{4}$$

Here $\delta\beta_p^{(0)}$, $\delta\beta_p^{(1)}$, and $\beta_p^{(2)}$ denote propagation constant mismatch, modal dispersion and chromatic dispersion, respectively. f_{pppp} and f_{ppii} are nonlinear coupling coefficients. Equation (4) includes intramodal nonlinear effect (first term in the right of equation) and intermodal nonlinearity among modes. If only nonlinear terms are considered, and the power of pulses is assumed as $P_p = 8|A_p|^2/9 + 4\sum_{i \neq p} f_{ppii} |A_i|^2/3 f_{pppp}$, the equation can be expressed just as [57]

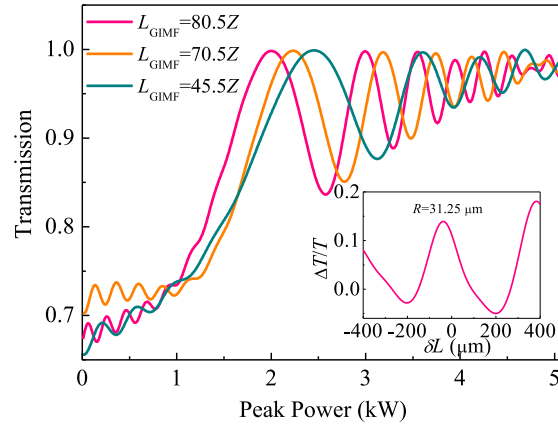$$\frac{\partial A_p}{\partial z} = \frac{in_2\omega_0 f_{pppp}}{c} P_p A_p. \tag{5}$$

Fig. 3. The dependence between transmission and peak power with $L_{GIMF} = 80.5Z$, 70.5Z and 45.5Z, where Z is oscillate period under linear case. Inset: relative change of transmission between nonlinear and linear case as a function of variation δL around $L_{GIMF} = 70.5Z$. In the simulation, the radius $R = 31.25$ μm and relative index difference between center and cladding of GIMF $\Delta = 0.029$.

Therefore, the field envelop after propagation z distance is easy to find,

$$A_p(z, t) = A_p(0, t) \exp\left(\frac{in_2\omega_0 f_{pppp}}{c}P_p z\right),$$
(6)

which indicates that nonlinear effects will lead to the accumulation of an additional phase shift along multimode fiber. In nonlinear limit, the oscillate period L_{NL-MMI} can be written as

$$L_{NL-MMI} = \frac{2\pi}{\delta\beta_p^{(0)} + n_2\omega_0 f_{pppp}(P_p - P_1)/c}.$$
(7)

For the sake of insight into saturable absorption of the all–fiber structure, behaviors of transmission and relative change of transmission ($\triangle T/T$) are discussed using the metrics in [58], as shown in Fig. 3. Fig. 3 displays that nonlinear modulation feature depends on intensity and multimode fiber length: 1) the rapid and damped oscillation of transmission proves (7), observing the diminution of L_{NL-MMI} with enhanced intensity. 2) Considering that the nonlinear phase is accumulated, demand of intensity for generating first peak in oscillation reduces with increase of L_{GIMF}, where L_{GIMF} is length of GIMF. 3) The relative transmission can be tuned by fine–tuning the length of GIMF, such as stretching or bending GIMF.

In order to achieve SA effect, a condition for achieving mode–locking is L_{GIMF} located at $(m + 0.5)$ Z or $m L_{NL-MMI}$, where m is an integer. In this condition, the transmission reaches a maximum for high power or minimum for low power, and SAs exhibit obvious intensity-dependent characterize.

2.2 Spectral Filtering Effect

NLMMI effect in multimode fiber displays a simple tunable mechanism of filtering. Based on (3), total coupling efficiency η can be written as $\eta = \sum_{k=0}^{g-1} \sum_{j=0}^{g-1} c_k^2 c_j^2 \exp[i(\beta_k - \beta_j)z]$, where the modified expansion coefficients c_k, c_j can be seen in [63]. It shows that η will reach a maximum value when the exponential term satisfies $\exp(i2\pi * q)$, confirming the function of filter. The power coupling efficiency or transmission from GIMF to SMF2 reaches a maximum value with the length of GIMF equal to the self-imaging distance L_{NL-MMI}, which is highly wavelength dependent. As the wavelength–mismatching in (7) increases, transmission decreases and the all–fiber structure in Fig. 2 exhibits a function of filter. The center wavelength of the filter is given as

$$\lambda_0 = q\frac{n_{GIMF}(2R)^2}{L_{GIMF}} \quad (q = 0, 1, 2, \ldots),$$
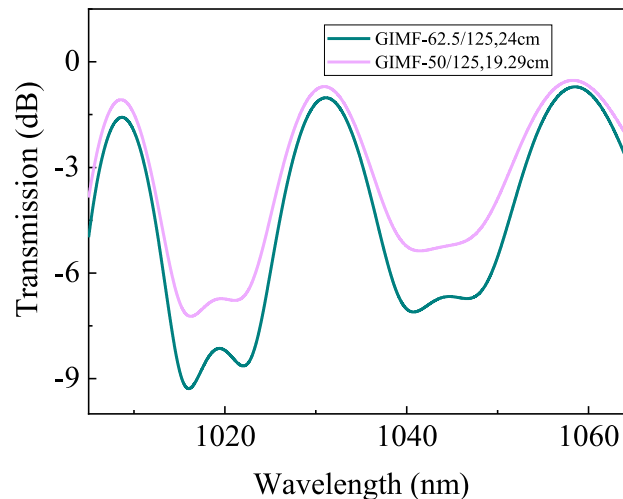(8)

Fig. 4. Filter bandwidths for two commercial GIMFs with different core radius and L_{GIMF}.

where q is the self–imaging number, n_{GIMF} denotes refractive index. Thus, fine–tuning of L_{GIMF} mirrors the tunable mechanism of filter. The simulated spectrum for a NLMMI–based filter can be seen in Fig. 4 [63], [64]. The behaviors of oscillations and gradual increase in minimum of transmission are contributed to wavelength dependence of $\triangle$ and mode field radium, which can be expressed by $y = y_0 + \delta(\lambda - \lambda_0)$. λ_0 is the center wavelength, and the factor of wavelength–dependence δ is fixed by fitting with experimental data. Fig. 4 indicates that the filter bandwidth can be optimized by varying core radius of GIMF. The bandwidth increases as the core radius of GIMF decreases. As describe in (3), the center wavelength of filter dependent on L_{GIMF} and a decrease of L_{GIMF} is needed to maintain the same filter center wavelength.

2.3 All–Fiber SAs Implementation

Because of oscillate period Z in GIMF being 100 μm scale, the demand for accuracy controlling L_{GIMF} is rigorous. In ultrafast fiber lasers, the all–fiber SAs have been implemented using three methods at present. One is to select a multimode fiber with larger oscillator period Z by virtue of the relationship between the oscillator period and core radium, such as SIMF, which possesses oscillator period Z of 10 mm scale and the lengths of SIMF are conveniently controlled with a fiber cleaver, as shown in Fig. 5(a) [57]. Another one is to fine–tuning L_{GIMF} by stretching the GIMF, as shown in Fig. 5(b) [65]. All–fiber SAs are fixed by fiber alignment state and tuned through precision translation stage to match the condition for mode–locking. The third one is to excite more high–order modes in multimode fiber through special design. Given the existence of high–order modes, the mode field distribution can be changed by introducing bends in device, leading to the ratio of fundamental mode coupling into following fiber varied. In the nonlinear limit, the intensity-dependent nonlinear effects affect oscillator period owing in GIMF. Therefore, introducing of bends varies the intensity-dependent transmission. Fig. 5(c) shows one designed SA implementation by inserting a piece of SIMF with the length of 328 μm, and bends are used to obtain efficient phase matching. Because of larger radius of SIMF, more higher-order modes will be excited when single-mode light is coupled into SIMF, and relative phase variations of the modes resulting from bending perturbation change the mode field distribution, which affects the coupling efficiency from GIMF to SMF and nonlinear strength. In other words, the intensity-dependent transmission could be achieved without accuracy controlling of L_{GIMF} [55], [56], [66].

The technique for charactering nonlinear transmission of all–fiber SAs is to alter pulse strength experiencing specimen by variable optical attenuator, as shown in Fig. 6. A 1570 nm pulsed fiber
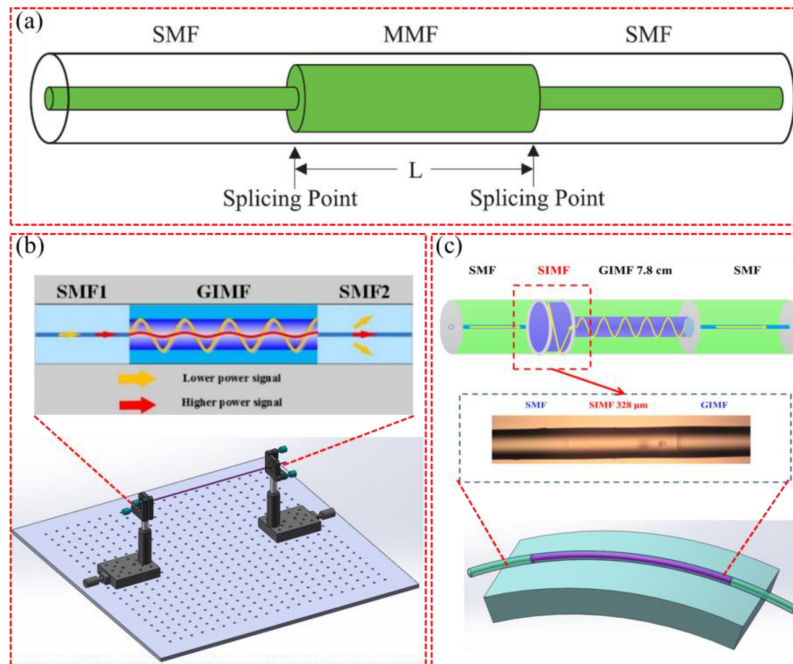
Fig. 5. Implementations of all-fiber SAs. (a) Using SIMF with large NLMMI period [57], (b) fine–tuning GIMF with precision translation stage [65], and (c) exciting more high–order modes by inserting a piece of SIMF with length of μm scale and introducing bends [67]. Figure (a) reproduced with permission from [57] © 2018 Photonics Research. [Adapted] with permission from [refs 65, 67] © The Optical Society.
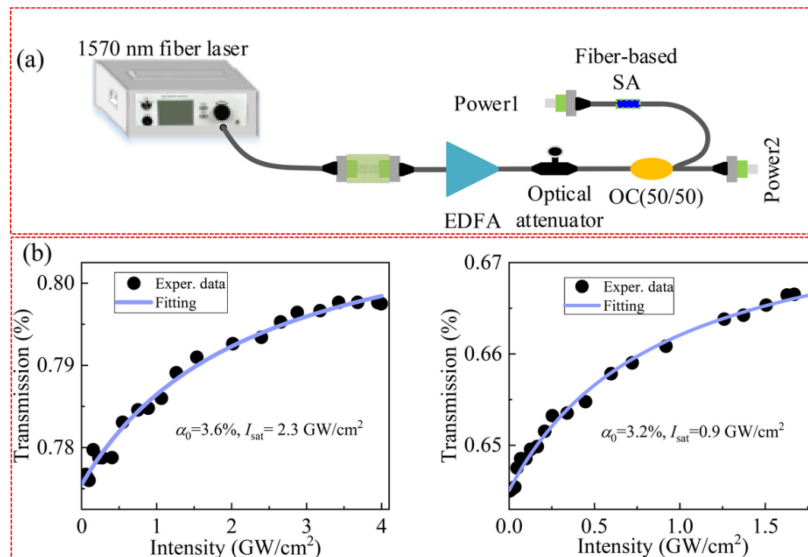
Fig. 6. Power-dependent characterization. (a) Schematic setup for measuring saturable absorption. (b) Nonlinear transmission curves of 23.5 cm GIMF SA at stretching lengths of 320 and 430 μm.

laser is divided into two equal arms and power meters work simultaneously in both output ports. The power–dependent transmission using the all–fiber SAs in Fig. 5(b) displays behaviors of saturable absorption and tunable characteristic.

Fig. 7. The achievements experimentally of Initial fiber lasers based on NLMMI effect. (a) Schematic setup of Q-switched fiber laser and (b) corresponding repetition rate and pulse duration as a function of pump power [54] [Reprinted] with permission from [ref 54] © The Optical Society. (c) Schematic setup of soliton fiber laser based on SIMF-GIMF SA, and corresponding autocorrelation trace and spectrum after amplification [55] (©[2017] IEEE).
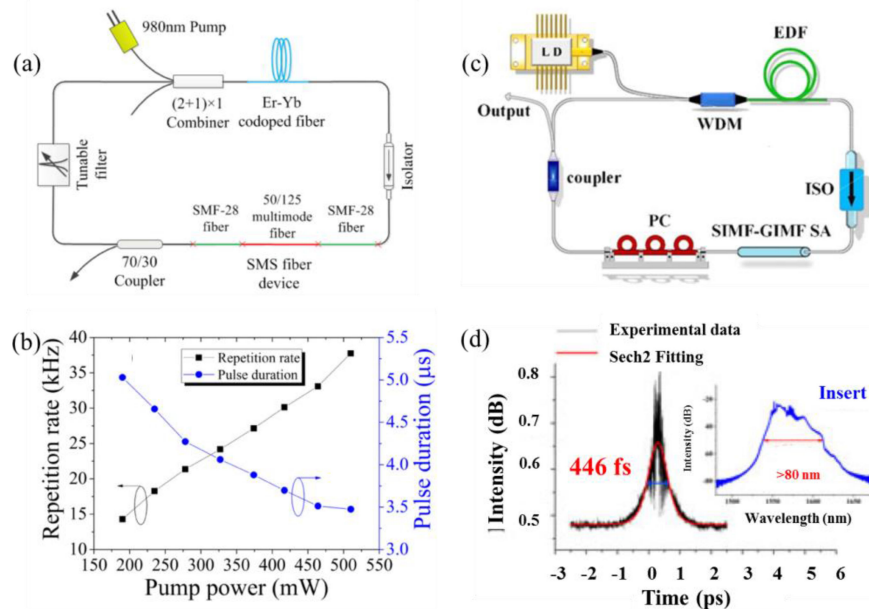
3. All–Fiber SAs For Ultrafast Fiber Lasers

The above nonlinear transmission features of all–fiber SAs motivate researchers to investigate their applications in ultrafast photonics, and the devices had been applied for ultrafast fiber lasers in wide wavelength regions covering 1, 1.55, and 2 μm.

3.1 Er–Doped Fiber Lasers

In 2015, the novel modulation mechanism based on the all–fiber SAs was firstly successfully used in ring fiber laser, and Q-switched pulses with maximum pulse energy of 0.78 μJ were obtained. Fig. 7(b) showed the repetition rate and pulse duration of the Q-switched fiber laser as a function of pump [54]. The results demonstrated that NLMMI–based structure using multimode fiber provided a new nonlinear effect to induce modulation mechanism in ultrafast fiber lasers. However, because of the short interference period, many samples were fabricated to select suitable one to achieve stable operation. Until 2017, SMF–SIMF–GIMF–SMF structure with 3.16% modulation depth was demonstrated, which excites more high-order modes to eliminate the limitation of L_{GIMF} [55], and soliton fiber laser centered at 1590 nm was achieved, as shown in Fig. 7(c) and (d). The mode–locked fiber laser possessed pulse duration of 446 fs and maximum pulse energy of 47 pJ. As the authors demonstrated, the output performance is affected by the length of SIMF and GIMF in [55]. The lengthening of SIMF leads to the single pulse energy decreased. And L_{GIMF} below a critical value will greatly hinder the promotion of output [55], [68].

After the soliton reported in [55] much attention has been paid to the all–fiber SA–based ultrafast fiber lasers. By introducing a microcavity with length of 45 μm, SMF-GIMF-SMF structure without stretching behaved saturable absorption with 1.9% modulation depth, as shown in Fig. 8(a) [69]. This structure eliminated effectively the demand of precisely process of L_{GIMF} and had a high stability for mode-locking operation at fundamental frequency. By increasing the pump power, harmonic mode-locking with a well-organized pulse train could also be achieved. Fig. 8(b) displayed the
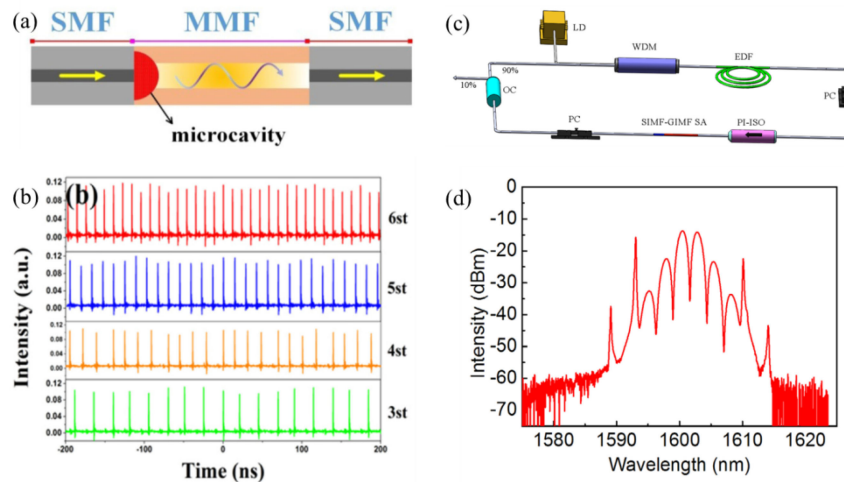
Fig. 8. Special multi-pulse fiber lasers. (a) The schematic diagram of SMF-GIMF-SMF structure with microcavity. (b) Pulse trains of harmonic mode-locking [69] [Reprinted] with permission from [ref 69] © The Optical Society. (c) Schematic setup of two-soliton bound fiber laser and (d) output spectrum [68] (Reproduced from [Fengyan Zhao, Hushan Wang, Xiaohong Hu, Yishan Wang Wei Zhang, Ting Zhang Chuandong Sun and Zhijun Yan, "Experimental observation of bound solitons with a nonlinear multimode interference-based saturable absorber," Laser Physics Letters, vol. 15, no. 11, Nov. 2018, Art. no. 115106.], with the permission of IOP Publishing).

harmonic mode–locking operation with maximum order of 6th achieved in this structure. Using SMF–SIMF–SMF structure, another special multi-pulse fiber laser has been achieved, as shown in Fig. 8(c) and (d) [68]. With suitable tuning of interaction potential through polarization controller, a set of two-soliton bound molecules possessing multiple discrete equilibrium distances were observed. Subsequently, studies demonstrated that dispersion governing fiber lasers using NLMMI–based SAs could also be acquired. The relationship between pulses and net cavity dispersion has been investigated using SMF–SIMF–SMF structure, and maximum pulse energy of 0.81 nJ was achieved in this mode–locked fiber laser [57]. However, because of the modifiable total cavity dispersion by dispersion engineering capabilities of higher-order modes and fluctuations in the process of transferring power between modes, the formation of dissipative soliton operating in normal dispersion region is hindered. When fiber lasers were constructed in the near zero region of cavity chromatic dispersion, two different mode–locking operations could be flexible switched by governing modal dispersion, and pulses with energy as high as 4 nJ have been generated in our previous work, as shown in Fig. 9(c) and (d) [58]. Of course, by varying the stretching length of GIMF, mode–locked fiber lasers behaving of wavelength-switchable operations could also been obtained [65].

Recently, dark pulse fiber lasers have been achieved using all–fiber SAs in our experiments, as shown in Fig. 10. The all–fiber SA was implemented using a SMF-GIMF-SMF structure with bends. When the pump power reached threshold and polarization controller state was suitable, dark pulses were achieved. Fig. 10(b) plotted the typical pulse sequences with 110 mW pump power. Pulse interval of 202 ns in Fig. 10(b) matches well with the cavity roundtrip time. The duration of pulse was about 10 ns. The 3 dB bandwidth of spectrum was 0.3 nm, as shown in Fig. 10(c). Clearly, the spectrum with two asymmetry peaks was observed, attributing to the spectral filtering effect within gain bandwidth which results from the SMF–GIMF–SMF structure [70], [71], as shown in Fig. 4.
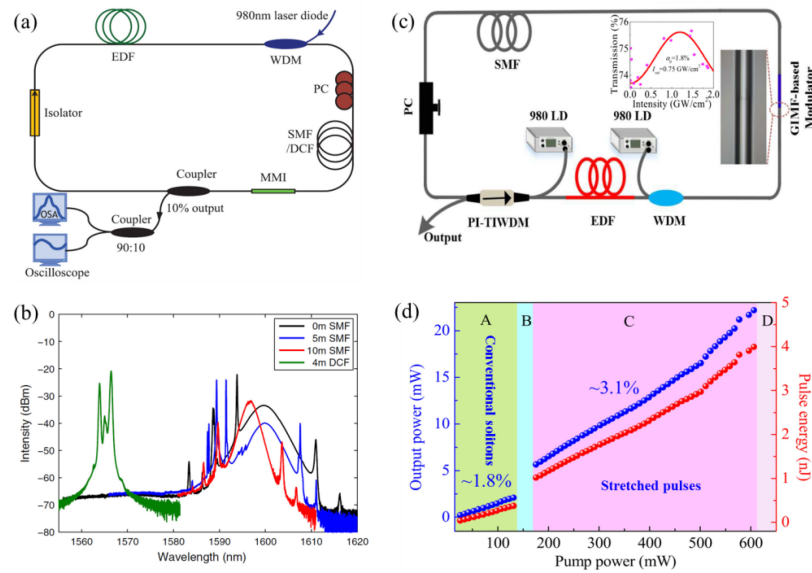
Fig. 9. Dispersion governing fiber lasers. (a) Schematic setup of Er-doped fiber laser based on SMF-SIMF-SMF structure, and (b) corresponding output spectra for adding different lengths of SMF or dispersion compensation fiber [57]. (c) Schematic setup of mode-locking operations switchable fiber laser with SMF-GIMF-SMF structure, and (d) corresponding output power and pulse energy as a function of pump power [58]. Figures reproduced with permission from [57], [58] © Photonics Research.
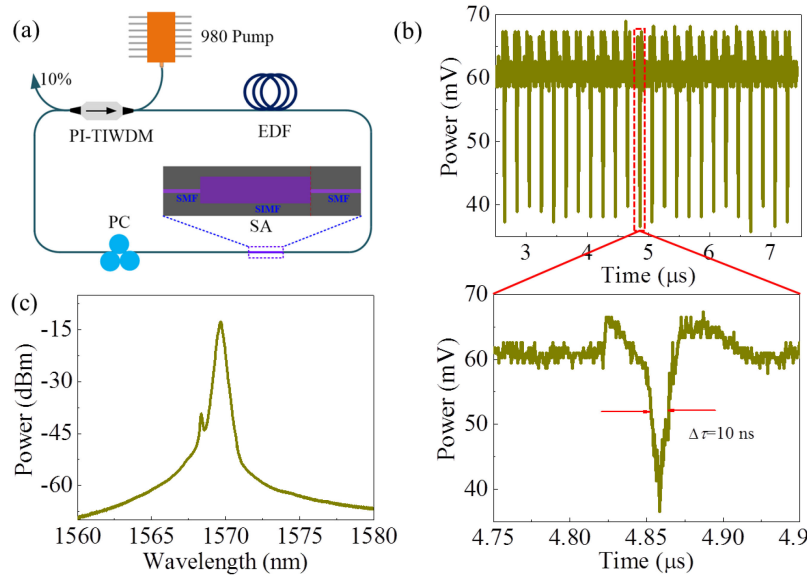
Fig. 10. Dark pulse fiber laser. (a) Schematic setup of fiber laser with SMF-GIMF-SMF structure. (b) Pulse sequences and pulse shape. (c) Output spectrum.

3.2 Yb–Doped Fiber Lasers

The first ytterbium–doped mode–locked fiber laser with an all–fiber based SA was demonstrated by Teğin and Ortaç [72]. The length of GIMF was selected as 14 cm to obtain 15 nm bandwidth of spectral filtering. The oscillator launched dissipative soliton at 1030 nm, possessing 0.13 nJ energy and 276 fs pulse duration, which was dechirped via an external grating compressor, as

Fig. 11. Dissipative soliton fiber laser. (a) Schematic setup with SIMF-GIMF structure. (b) Output dissipative soliton spectrum at 1030 nm. (c) Autocorrelation trace [72] [Reprinted] with permission from [ref 72] © The Optical Society.
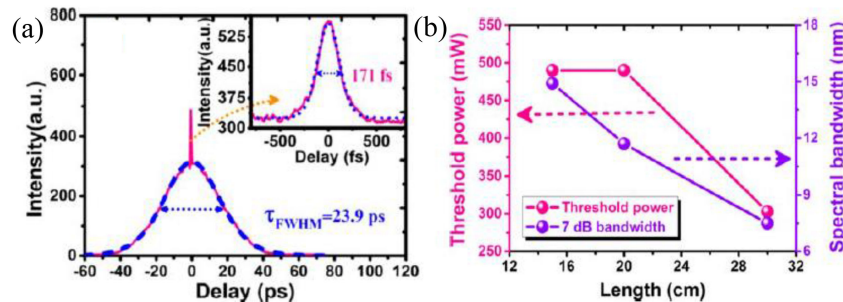
Fig. 12. Performance of noise-like pulse. (a) Autocorrelation trace, and (b) variation tendency of mode-locking threshold and spectral bandwidth as a function of increment of the length of GIMF [73]. Copyright (2018) The Japan Society of Applied Physics.

shown in Fig. 11. The presented fiber laser had high stability and could find applications in optical metrology and supercontinuum generation. Later, noise-like pulses in ring fiber laser based on SIMF–GIMF structure were presented, which had high average power of 279 mW at 41 MHz repetition rate [73]. As shown in Fig. 12(a), the pulse had 150 ps duration with fs–scale spike located on the top. Fig. 12(b) showed that this operation performance could be effectively controlled by optimizing the length of GIMF, such as pulse width and mode–locking threshold. Besides the SIMF–GIMF structure, embedding microcavity or offset splicing two kinds GIMF technologies could also excite high-order modes and has been used to achieve mode-locking operations [74], [75]. In the 1 μm region, the all–fiber SAs have been used not only for mode–locking but Q-switching operations [76].

3.3 Tm–Doped Fiber Lasers

By selecting suitable length of multimode fiber, a spectral overlap between transmission peak of multimode fiber-based structure and gain peak of Tm–doped fiber could be obtained. In the year of 2018, a Tm–doped mode-locked fiber laser based on NLMMI effect was demonstrated by Li [67]. The setup of Tm–doped fiber laser with 19.82 MHz repetition frequency could be seen in Fig. 13(a). The output spectrum has a 3 dB bandwidth of 3.6 nm, as shown in Fig. 13(b). The generated soliton centered at 1888 nm had 1.4 ps pulse duration and maximum average output
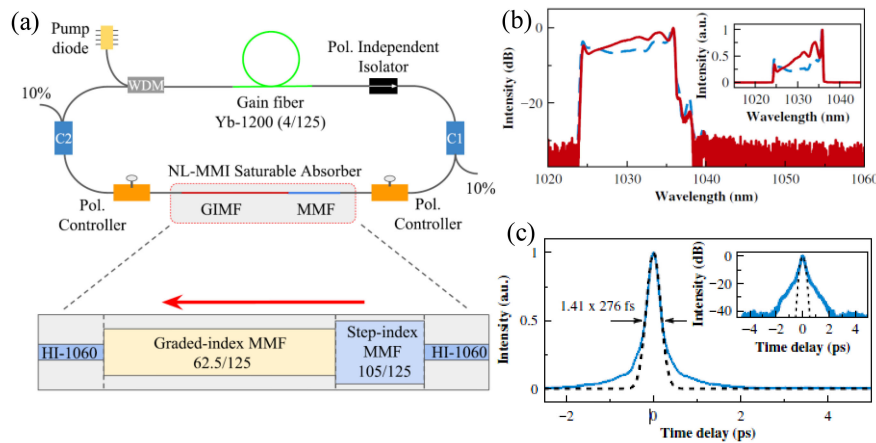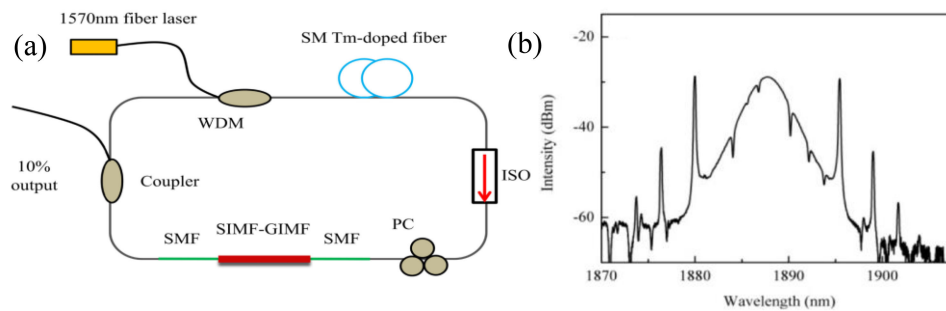
Fig. 13. Tm-doped fiber laser. (a) Schematic setup with SIMF-GIMF structure. (b) Output spectrum of conventional soliton at 1888 nm [67] [Reprinted] with permission from [ref 67] © The Optical Society.

power of 9 mW. As mentioned above, a multimode fiber based device could behave as a NLMMI–based filter to tune laser. And, considering the relationship between length of multimode fiber and strain $\Delta L = L\,\varepsilon + \alpha L\,\Delta T$, where ε and α denoted strain, temperature coefficient, respectively, a simple multiwavelength fiber laser could be achieved by strain. Inserting a rotary fiber squeezer in center portion of multimode fiber to provide tensile stress, a Tm-doped fiber laser with tunable multiwavelength ranging from 1892 to 1916 nm was proposed [77]. The 3 dB linewidth of tunable multiwavelength fiber laser was less than 0.04 nm and side mode suppression rations was about 54 dB.

4. Rogue Wave for Generating High-Energy Pulses

It evidences that principal modes (PMs), analogous to the two orthogonal modes in single-mode fiber, will be excited in multimode fiber by adjusting the polarization states. The group delay induced by PMs and mode coupling in multimode fiber can be modified through PC [78], [79]. Therefore, mode-locking operation regimes in fiber lasers are controllable due to group delay induced by PMs in multimode fiber. As demonstrated in our previous work, mode-locking operation's transition occurs in the all-fiber SA-based fiber laser [58]. A remarkable phenomenon is that a "gap" exists between the two mode–locking operations, which plays a vital in generating high–energy pulse, as the region B shown in Fig. 9(d). When the operation lies in B region, unstable multipulse generates. However, a fancy nonlinear phenomenon, optical rogue wave could be generated with suitable polarization states in B region.

In order to capture and gain insight into optical rogue wave, here, a powerful method for continuous single–shot measurement, dispersive Fourier transformation (DFT) technique has been applied. Using DFT, an analog in time domain of far–field diffraction of a spatial pattern, occurs when optical waveform experiences enough dispersion and reproduction of optical spectrum in the temporal waveform is observed [80]–[83]. DFT provides an effective method for capturing fast non–repetitive and rapid varying events and has been applied to spectroscopy, laser scanning and imaging.

As shown in Fig. 14, three features of optical rogue wave are observed [58], [84]–[86]: First, the maximum intensity of rogue pulse exceeds significant wave height (SWH) calculated as 0.9 by a factor of 2.5. Second, the dynamics process shows that appearance and annihilation of the events are spontaneous, meaning the limited lifetime of events. Third, the statistical distribution is L–shaped with long tails. The rogue wave observed in region B mirrors the laser physics of generating a high–energy pulse from a relative low-energy pulse, which is one of ultimate methods to govern the generation of high–energy pulse in modern optics. In general, optical rogue wave in fiber lasers arises from energy transfer and the peak power of rogue wave can be controlled by varying laser gain.

However, adjusting polarization controller states only, the generation of rare events can be managed flexibly in our experiments, as shown in Fig. 15. With suitable states of polarization con-
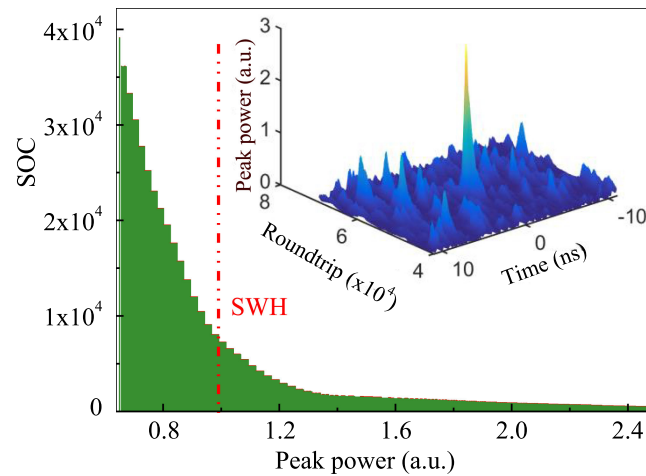
Fig. 14. Statistical of occurrence (SOC) of pulse peak power. Inset: the dynamics process of an optical rogue wave [58]. Figure reproduced with permission of Photonics Research.
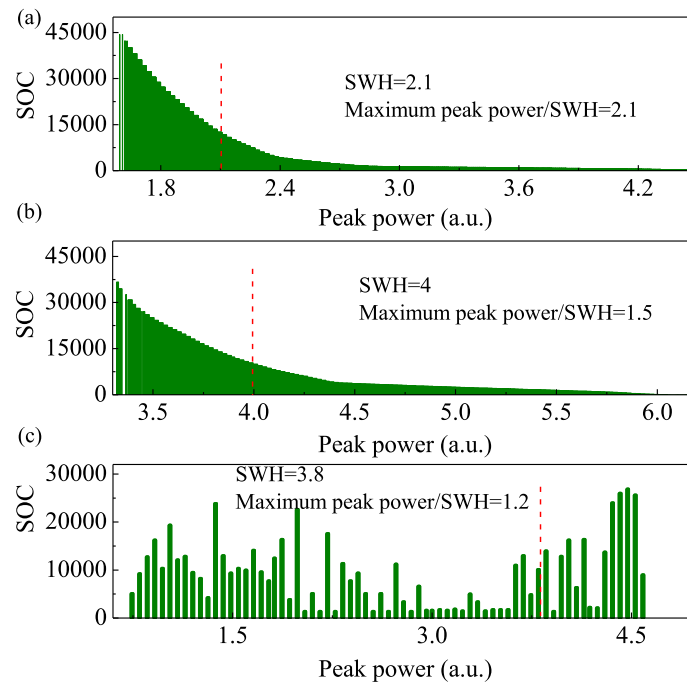
Fig. 15. SOC of pulse peak power under different polarization states. The statistic features of L-shape with long tails vanish gradually from (a) to (c). The red dash line denotes SWH value.

troller, the ratio of rogue wave between maximum peak power and SWH decreases, as shown in Fig. 15(a). The ratio reduces below 2 when the polarization state is varied discontinuously, as shown in Fig. 15(b) and (c). It notices that the event in Fig. 15(b) possesses an L-shape of statistic histogram but a ratio of 1.5, which does not represent an optical rogue wave [85], [86].

Considering the experimental conditions, polarization mode dispersion (PMD) is attributed to the tuning of rogue wave. Here, a modified nonlinear Schrödinger equation is applied to describe these nonlinear behaviors [85], [86]. And, the coupling between two polarization components of pulse can
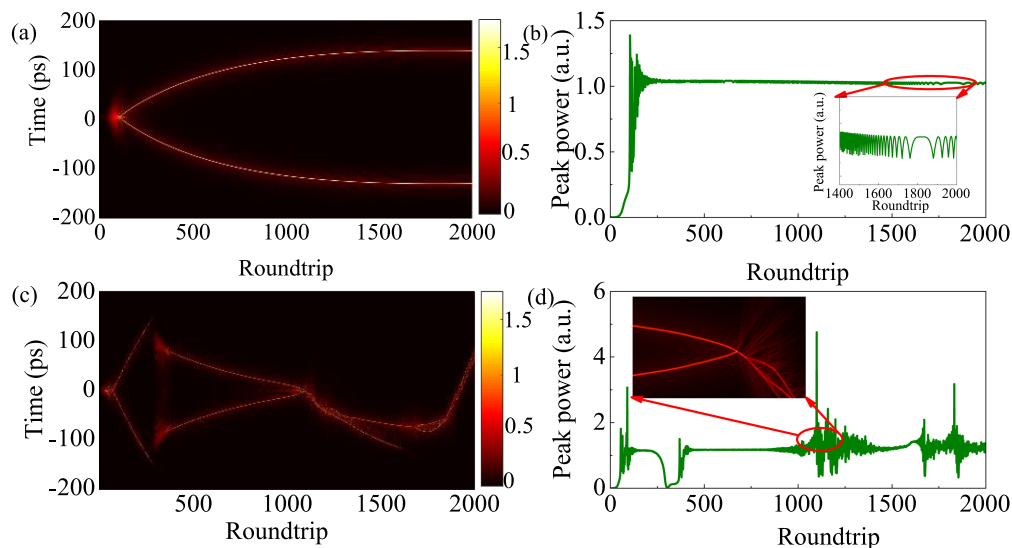
Fig. 16. Simulation results. Temporal dynamic (a) and (b) output peak power without PMD. (c) Pulse evolution and (d) the record of rare events with PMD = 0.065 ps.

be expressed by coupling coefficient κ, relative phase φ_1 and cross phase φ_2,

$$R = \begin{bmatrix} (1-\kappa)\ \exp(i\varphi_1) & \kappa\ \exp(i\varphi_2) \\ \kappa\ \exp(-i\varphi_2) & (1-\kappa)\ \exp(-i\varphi_1) \end{bmatrix}. \tag{9}$$

The temporal dynamics and output peak power without PMD are displayed in Fig. 16. In this case, fiber laser operates in unstable two–pulse region, where pulse power behaves an oscillation nearby the stationary value, as shown in Fig. 16(a) and (b). However, when the PMD is taken into account, asymmetric instabilities occur and pulse evolves into chaos state. When the PMD is set as 0.065 ps in simulation, pulse dynamics behave obvious change and the peak power within 2000 continuous roundtrips appears sudden rises, which can be seen in Fig. 16(c) and (d). The maximum ratio between peak power and significant wave height is 2.8. It notices that a sudden rise of pulse amplitude occurs when pulses encounter during propagation.

The statistic histograms of pulse with the same parameters but different PMD are shown in Fig. 17. For the region of two–pulse without interaction, pulse dynamics does not enable the existence of higher field intensity than 1.6. Once variation of PMD appears, dynamics are perturbed and pulse intensities are enhanced. The plots demonstrate that the significant roles of PMD are played in the generation process of rare events.

Because of the presentation of polarization mode dispersion, the drift velocity of localized wavepacket characterizing instability dynamics is modulated and the perturbation evolves into asymmetric instability [87]–[89]. Thus, the system is sensitive to noise. The collision between two or more solitons appears in the unstable region during pulses propagation, where the amplitude of one pulse enhances from relative low ones and optical rogue wave occurs.

5. Conclusion and Perspective

In this Review, the fundamental theory, the fundamental theory, implementation scenarios, and ultrafast fiber lasers of the recent advances using NLMMI-based all-fiber SAs are summarized. A special attention is paid on optical rogue waves in the all-fiber SA-based ultrafast fiber lasers, which reveals the laser physics behind the dynamics for generating high-energy pulses and directs the design of high-energy ultrafast fiber lasers.
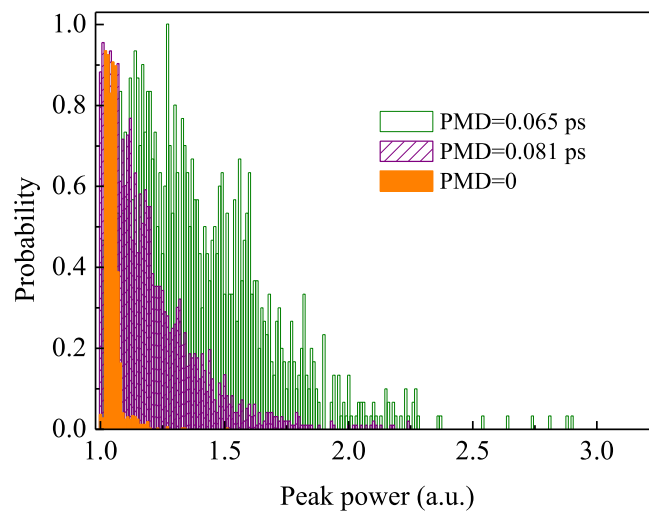
Fig. 17. Simulation results. Statistic information of pulse with PMD = 0, 0.065 and 0.081 ps.

5.1 Challenges and Potential Solutions

The NLMMI-based all-fiber SAs exhibit intriguing properties, especially in easy to integrate and high damage threshold. However, challenges presented in the technology are needed to be solved urgently.

In the multimode fiber, quasi-degenerate modes, having very close propagation constant, are sensitive to perturbation of bending, index variation and temperature [90], [52]. The fiber lasers based on multimode fiber are absence of environmental stability. An environmentally stable cavity with Faraday rotator and fibers with extremely large mode areas would provide a promising solution to be immune to distortion induced by external environmental factors [91], [92]. In this structure, linear phase drifts related to polarization are eliminated and the variation of nonlinear phase is immune to environmental changes [93]. Sigma-type cavity, containing linear and ring segments, could also be a possible solution. The hybrid design is constructed by polarization maintaining fiber and Faraday mirror to retain environmental stability [94], [95]. Additionally, it will be a potential solution of modal dispersion management to modify the net modal dispersion to the demands, such as using multicore fiber to reverse modal dispersion [96], fiber Bragg gratings or inhomogeneous nanostructures to separate propagation length of modes [97].

And, what a complex dynamic exists among the generation of ultrafast pulses in fiber lasers based on NLMMI effects? Several ultrafast fiber lasers have been implemented based on multimode fiber, however, as demonstrated above, stable dissipative soliton fiber lasers with normal dispersion in 1.55 μm region are difficult to achieve using the all-fiber SAs. What new nonlinear phenomenon will occur during the dynamics? These issues are urgently demanded to seek an efficient controlling technique to acquire expected ultrafast pulses. Our previous work demonstrated that the dynamics of mode-locking without beating are significant different from that in single-mode fiber laser [58]. Besides, it is worthwhile to explore the new physics in multimode fiber lasers and seek potential applications, for example, vortex formation, wave turbulence, disorder during the linear and nonlinear propagation [98], [52].

In addition, owing to large mode mismatch between GIMF and SMF, large insertion loss of such a SA will be introduced into fiber laser. And the threshold of self-starting mode-locking is higher than that of based on standard single fiber [99], [58]. Ultra-high numerical aperture (UHNA) fiber may be useful as bridge fiber between high NA and single-mode fibers. However, a large extra dispersion and reduced self-start capacity should be considered. As Mafi *et al.* demonstrated, by incorporating a section of large mode area fiber (such as Corning LMA-20), ultra-low-loss coupling

could be achieved in all-fiber SAs. To implement this purpose, the length of GIMF should be set at an optimal value [64].

5.2 Perspectives and Applications

The existence of oscillate modes and self–imaging effect reduce the effective nonlinear coefficient, and the tolerance of pulse energy in fiber laser increases. Benefiting from these advantages, SMF–MMF–SMF structure provides a promising solution for scaling up peak power and pulse energy in mode–locked fiber lasers. With large fiber core diameter, fiber laser based on NLMMI would possess the capable of generating ultrafast pulses with millijoule pulse energy. Beyond the wavelength regions mentioned above, mode-locking fiber lasers based on NLMMI operating in mid-infrared region will be more exciting. Comparing with the lasers in near-infrared, mid-infrared fiber lasers have fascinating characters of higher output power and devices for modal-dispersion management [100], [101]. Considering existence of modes competition in multimode fiber, the mentioned fiber lasers with a high spectral quality can be obtained by nonlinear spectral compression, such as using bends, long–period fiber gratings, and introducing side–core [102], [103].

Recently, interactions between modes have been applied in microcavity to generate frequency combs and novel solitons [104]–[106]. Furthermore, μm-scale laser resonators were demonstrated to own the ability of control oscillating of modes, which provide a promising solution of high integration [107], [108]. The microring lasers combine the superiorities of compact structure and multimode cavity. Therefore, it is potential and exciting that the μm-scale ultrafast lasers based on NLMMI effect are implemented in future. The on-chip multimode lasers, generating ultrafast pulses, broadband combs and supercontinuum, can pave the way for photonic integrated circuits and next-generation optoelectronic devices in communications and information processing.

In addition, owing to the polarization-related mode-locking, electrical polarization control has been the focus of attention for automatic mode-locking. Intelligent programmable fiber lasers based on NLMMI effect will be another trend in future. Enriched physics and complexity in multimode fiber provide diverse solutions to control the operation of fiber laser based on NLMMI effect. The intelligent lasers could exhibit superior performance of high stability, ultrafast response and versatility, showing potential for practical applications in engineering and scientific research.

References

[1] L. Khaykovich *et al.*, "Formation of a matter-wave bright soliton," *Science*, vol. 296, no. 5571, pp. 1290–1293, May 2002.
[2] N. Zabusky and M. Kruskal, "Interaction of 'solitons' in a collisionless plasma and the recurrence of initial states," *Phys. Rev. Lett.*, vol. 15, no. 6, pp. 240–243, Aug. 1965.
[3] W. H. Renninger and F. W. Wise, "Optical solitons in graded-index multimode fibers," *Nat. Commun.*, vol. 4, Apr. 2013, Art. no. 1719.
[4] G. P. Agrawal, *Nonlinear Fiber Optics*. San Francisco, CA, USA: Academic Press, 2007.
[5] A. J. Aemaria, D. A. Stetser, and H. Heynau, "Self mode-locking of lasers with saturable absorbers," *Appl. Phys. Lett.*, vol. 8, no. 7, pp. 174–176, 1966.
[6] A. Hasegawa and F. Tappert, "Transmission of stationary nonlinear optical pulses in dispersive dielectric fibers. I. Anomalous dispersion," *Appl. Phys. Lett.*, vol. 23, no. 3, pp. 142–144, Aug. 1973.
[7] A. Hasegawa, "Soliton-based optical communications: An overview," *IEEE J. Sel. Topics Quantum Electron.*, vol. 6, no. 6, pp. 1161–1172, Nov.–Dec. 2000.
[8] F. W. Wise, A. Chong, and W. H. Renninger, "High-energy femtosecond fiber lasers based on pulse propagation at normal dispersion," *Laser Photon. Rev.*, vol. 2, no. 1–2, pp. 58–73, Apr. 2008.
[9] U. Keller, "Recent developements in compact ultrafast lasers," *Nature*, vol. 424, pp. 831–838, Aug. 2003.
[10] E. F. Martin and H. Ingmar, "Ultrafast fiber lasers," *Nature Photon.*, vol. 7, pp. 868–874, Oct. 2013.
[11] X. K. Franz *et al.*, "Control of solid state laser dynamics by semiconductor devices," *Opt. Eng.*, vol. 34, no. 7, pp. 2024–2036, Jul. 1995.
[12] C. Hönninger, R. Paschotta, F. Morier-Genoud, M. Moser, and U. Keller, "Q-switching stability limits of continuous-wave passive mode locking," *J. Opt. Soc. Am. B*, vol. 16, no. 1, pp. 46–56, Jan. 1999.
[13] Z. Sun, A. Martinez, and F. Wang, "Optical modulators with 2D layered materials," *Nature Photon.*, vol. 10, pp. 227–238, Mar. 2016.
[14] R. N. Zitter, "Saturated optical absorption through band filling in semiconductors," *Appl. Phys. Lett.*, vol. 14, pp. 73–75, Oct. 1969.

[15] E. Garmire, "Resonant optical nonlinearities in semiconductors," *IEEE J. Select. Topics Quantum Electron.*, vol. 6, no. 6, pp. 1094–1100, Nov.–Dec. 2000.

[16] O. Okhotnikov, A. Gurdinim, and M. Pessa, "Ultra-fast fiber laser systems based on SESAM technology: new horizons and applications," *New J. Phys.*, vol. 6, no. 1, p. 177, Nov. 2004.

[17] M. Haiml *et al.*, "Optical nonlinearity in low-temperature-grown GaAs: Microscopic limitations and optimization strategies," *Appl. Phys. Lett.*, vol. 74, no. 21, pp. 3134–3136, May 1999.

[18] U. Keller *et al.*, "Semiconductor saturable absorber mirrors (SESAMs) for femtosecond to nanosecond pulse generation in solid-state lasers," *IEEE J. Sel. Topics Quantum Electron.*, vol. 2, no. 3, pp. 435–453, Sep. 1996.

[19] L. A. Gomes, L. Orsila, T. Jouhti, and O. G. Okhotnikov, "Picosecond SESAM-based ytterbium mode-locked fiber lasers," *IEEE J. Sel. Topics Quantum Electron.*, vol. 10, no. 1, pp. 129–136, Apr. 2004.

[20] O. G. Okhotnikov, T. Jouhti, J. Konttinen, S. Karirinne, and M. Pessa, "1.5 μm monolithic GaInNas semiconductor saturable-absorber mode locking of an erbium fiber laser," *Opt. Lett.*, vol. 28, no. 5, pp. 364–366, Mar. 2003.

[21] Z. C. Luo, A. P. Luo, and W. C. Xu, "Tunable and switchable multiwavelength passively mode-locked fiber laser based on SESAM and inline birefringence comb filter," *IEEE Photon. J.*, vol. 3, no. 1, pp. 64–70, Dec. 2010.

[22] A. Rutz, R. Grange, V. Liverini, M. Haiml, S. Schon, and U. Keller, "1.5 μm GaInNAs semiconductor saturable absorber for passively mode-locked solid-state lasers," *Electron. Lett.*, vol. 41, no. 6, pp. 321–323, Apr. 2005.

[23] S. Iijima and T. Ichihashi, "Single-shell carbon nanotubes of 1-nm diameter," *Nature*, vol. 363, pp. 603–605, 1993.

[24] H. Kataura *et al.*, "Optical properties of single-wall carbon nanotubes," *Synth. Met.*, vol. 103, no. 1–3, pp. 2555–2558, Jun. 1999.

[25] G. W. Chen, W. L. Li, H. R. Yang, and Y. C. Kong, "Switchable dual-wavelength fiber laser mode-locked by carbon nanotubes," *J. Modern Opt.*, vol. 62, no. 5, pp. 353–357, Jun. 2015.

[26] W. Li and G. Chen, "Single-wavelength-tunable and dual-wavelength-switchable Tm-doped fiber soliton laser based on single-walled carbon nanotubes," *Modern Phys. Lett. B*, vol. 33, no. 11, Apr. 2019, Art. no. 1950136.

[27] S. Y. Set *et al.*, "Mode-locked fiber lasers based on a saturable absorber incorporating carbon nanotubes," in *Proc. Opt. Fiber Commun. Conf.*, Optical Society of America, 2003, PD44.

[28] M. Chernysheva *et al.*, "Carbon nanotubes for ultrafast fibre lasers," *Nanophotonics*, vol. 6, no. 1, pp. 1–30, Jan. 2017.

[29] L. Yun, "Generation of vector dissipative and conventional solitons in large normal dispersion regime," *Opt. Exp.*, vol. 25, no. 16, pp. 18751–18759, Aug. 2017.

[30] M. Liu, A. P. Luo, W. C. Xu, and Z. C. Luo, "Dissipative rogue waves induced by soliton explosions in an ultrafast fiber laser," *Opt. Lett.*, vol. 41, no. 17, pp. 3912–3915, Sep. 2016.

[31] K. S. Novoselov *et al.*, "Electric field effect in atomically thin carbon films," *Science*, vol. 36, no. 5696, pp. 666–669, Oct. 2004.

[32] Q. Bao *et al.*, "Atomic-layer graphene as a saturable absorber for ultrafast pulsed lasers," *Adv. Funct. Mater.*, vol. 19, no. 19, pp. 3077–3083, Oct. 2009.

[33] H. Zhang, Q. Bao, D. Tang, L. Zhao, and K. Loh, "Large energy soliton erbium doped fiber laser with a graphene-polymer composite mode locker," *Appl. Phys. Lett.*, vol. 95, no. 14, Oct. 2009, Art. no. 141103.

[34] J. Bogustawski *et al.*, "Graphene actively mode-locked lasers," *Adv. Funct. Mater.*, vol. 28, May 2018, Art. no. 1801539.

[35] L. Yun *et al.*, "PbS quantum dots as a saturable absorber for ultrafast laser," *Photon. Res.*, vol. 6, no. 11, pp. 1028–1032, Nov. 2018.

[36] Y. Ge *et al.*, "Broadband nonlinear photoresponse of 2D TiS2 for ultrashort pulse generation and all-optical thresholding devices," *Adv. Opt. Mater.*, vol. 6, Dec. 2018, Art. no. 1701166.

[37] D. Mao *et al.*, "WS$_2$ saturable absorber for dissipative soliton mode locking at 1.06 and 1.55 μm," *Opt. Exp.*, vol. 23, no. 21, pp. 27509–27519, Oct. 2015.

[38] J. Liu, Y. Chen, Y. Li, H. Zhang, S. Zheng, and S. Xu, "Switchable dual-wavelength Q-switched fiber laser using multilayer black phosphorus as a saturable absorber," *Photon. Res.*, vol. 6, no. 3, pp. 198–203, Mar. 2018.

[39] L. Yun, "Black phosphorus saturable absorber for dual-wavelength polarization-locked vector soliton generation," *Opt. Exp.*, vol. 25, no. 26, pp. 32380–32385, Dec. 2017.

[40] D. Mao *et al.*, "Broadband polarization-insensitive saturable absorption of Fe$_2$O$_3$ nanoparticles," *Nanoscale*, vol. 10, no. 45, pp. 21219–21224, Oct. 2018.

[41] X. D. Wang, Z. C. Luo, H. Liu, M. Liu, A.-P. Luo, and W.-C. Xu, "Microfiber-based gold nanorods as saturable absorber for femtosecond pulse generation in a fiber laser," *Appl. Phys. Lett.*, vol. 105, no. 16, Oct. 2014, Art. no. 161107.

[42] D. Mao *et al.*, "Ultrafast all-fiber based cylindrical-vector beam laser," *Appl. Phys. Lett.*, vol. 110, no. 2, Jan. 2017, Art. no. 021107.

[43] W. Li, G. Chen, G. Wang, C. Zeng, and W. Zhao, "Wideband wavelength-tunable ultrafast fiber laser based on black phosphorus saturable absorber," *Laser Phys. Lett.*, vol. 15, no. 12, Oct. 2018, Art. no. 125102.

[44] G. Wang, G. Chen, W. Li, W. Zhang, C. Zeng, and W. Zhao, "Indium selenide as a saturable absorber for a wavelength-switchable vector-soliton fiber laser," *Opt. Mater. Exp.*, vol. 9, no. 2, pp. 449–456, Feb. 2019.

[45] R. H. Stolen, J. Botineau, and A. Ashkin, "Intensity discrimination of optical pulses with birefringent fibers," *Opt. Lett.*, vol. 7, no. 10, pp. 512–514, Oct. 1982.

[46] D. Y. Tang, L. M. Zhao, B. Zhao, and A. Q. Liu, "Mechanism of multisoliton formation and soliton energy quantization in passively mode-locked fiber lasers," *Phys. Rev. A*, vol. 72, no. 4, Oct. 2005, Art. no. 043816.

[47] E. A. Kuzin, N. Korneev, J. W. Haus, and B. Ibarra-Escamilla, "Theory of nonlinear loop mirrors with twisted low-birefringence fiber," *J. Opt. Soc. Am. B*, vol. 18, no. 7, pp. 919–925, Jul. 2001.

[48] N. J. Doran and D. Wood, "Nonlinear-optical loop mirror," *Opt. Lett.*, vol. 13, no. 1, pp. 56–58, Jan. 1988.

[49] M. E. Fermann, F. Haberl, M. Hofer, and H. Hochreiter, "Nonlinear amplifying loop mirror," *Opt. Lett.*, vol. 15, no. 13, pp. 752–754, Jul. 1990.

[50] O. Pottiez, E. A. Kuzin, B. Ibarra-Escamilla, J. T. Camas-Anzueto, and F. Gutierrez-Zainos, "Experimental demonstration of NOLM switching based on nonlinear polarisation rotation," *Electron. Lett.*, vol. 40, no. 14, pp. 892–894, Jul. 2004.

[51] E. Nazemosadat and A. Mafi, "Nonlinear multimodal interference and saturable absorption using a short graded-index multimode optical fiber," *J. Opt. Soc. Amer. B*, vol. 30, no. 5, pp. 1357–1367, May 2013.

[52] L. G. Wright *et al.*, "Multimode nonlinear fiber optics: Massively parallel numerical solver, tutorial, and outlook," *IEEE J. Sel. Topics Quantum Electron.*, vol. 24, no. 3, pp. 1–16, Dec. 2018.

[53] J. Proctor and J. N. Kutz, "Nonlinear mode-coupling for passive modelocking: Application of waveguide arrays, dual-core fibers, and/or fiber arrays," *Opt. Exp.*, vol. 13, no. 22, pp. 8933–8950, Oct. 2005.

[54] S. Fu *et al.*, "Passive Q-switching of an all-fiber laser induced by the Kerr effect of multimode interference," *Opt. Exp.*, vol. 23, no. 13, pp. 17255–17262, Jun. 2015.

[55] Z. Wang *et al.*, "Er-doped mode-locked fiber laser with a hybrid structure of a step-index–graded-index multimode fiber as the saturable absorber," *J. Lightw. Technol.*, vol. 35, no. 24, pp. 5280–5285, Dec. 2017.

[56] U. Teğin and B. Ortaç, "All-fiber all-normal-dispersion femtosecond laser with a nonlinear multimodal interference-based saturable absorber," *Opt. Lett.*, vol. 43, no. 7, pp. 1611–1614, Apr. 2018.

[57] T. Chen, Q. Zhang, Y. Zhang, X. Li, H. Zhang, and W. Xia, "All-fiber passively mode-locked laser using nonlinear multimode interference of step-index multimode fiber," *Photon. Res.*, vol. 6, no. 11, pp. 1033–1039, Nov. 2018.

[58] G. Chen, W. Li, G. Wang, W. Zhang, C. Zeng, and W. Zhao, "Generation of coexisting high-energy pulses in a mode-locked all-fiber laser with a nonlinear multimodal interference technique," *Photon. Res.*, vol. 7, no. 2, pp. 187–192, Feb. 2019.

[59] L. G. Wright, D. N. Christodoulides, and F. W. Wise, "Controllable spatiotemporal nonlinear effects in multimode fibers," *Nature Photon.*, vol. 9, no. 5, pp. 306–310, Apr. 2015.

[60] M. Conforti, C. M. Arabi, A. Mussot, and A. Kudlinski, "Fast and accurate modeling of nonlinear pulse propagation in graded-index multimode fibers," *Opt. Lett.*, vol. 42, no. 19, pp. 4004–4007, Oct. 2017.

[61] S. Mumtaz, R. J. Essiambre, and G. P. Agrawal, "Nonlinear propagation in multimode and multicore fibers: Generalization of the Manakov equations," *J. Lightw. Technol.*, vol. 31, no. 3, pp. 398–406, Dec. 2012.

[62] A. Mecozzi, C. Antonelli, and M. Shtaif, "Coupled Manakov equations in multimode fibers with strongly coupled groups of modes," *Opt. Exp.*, vol. 20, no. 21, pp. 11673–11678, Oct. 2012.

[63] W. S. Mohammed and P. W. E. Smith, "All-fiber multimode interference bandpass filter," *Opt. Lett.*, vol. 31, no. 17, pp. 2547–2549, Sep. 2006.

[64] A. Mafi, P. Hofmann, C. J. Salvin, and A. Schülzgen, "Low-loss coupling between two single-mode optical fibers with different mode-field diameters using a graded-index multimode optical fiber," *Opt. Let.*, vol. 36, no. 18, pp. 3596–3598, Sep. 2011.

[65] Z. Wang *et al.*, "Stretched graded-index multimode optical fiber as a saturable absorber for erbium-doped fiber laser mode locking," *Opt. Lett.*, vol. 43, no. 9, pp. 2078–2082, May 2018.

[66] C. K. Asawa and H. F. Taylor, "Propagation of light trapped within a set of lowest-order modes of graded-index multimode fiber undergoing bending," *Appl. Opt.*, vol. 39, no. 13, pp. 2029–2037, May 2000.

[67] H. Li, Z. Wang, C. Li, J. Zhang, and S. Xu, "Mode-locked Tm fiber laser using SMF-SIMF-GIMF-SMF fiber structure as a saturable absorber," *Opt. Exp.*, vol. 25, no. 22, pp. 26546–26553, Oct. 2017.

[68] F. Zhao *et al.*, "Experimental observation of bound solitons with a nonlinear multimode interference-based saturable absorber," *Laser Phys. Lett.*, vol. 15, no. 11, Oct. 2018, Art. no. 115106.

[69] F. Yang *et al.*, "Saturable absorber based on a single mode fiber–graded index fiber–single mode fiber structure with inner micro-cavity," *Opt. Exp.*, vol. 26, no. 2, pp. 927–934, Jan. 2018.

[70] W. Liu *et al.*, "Dark solitons in WS$_2$ erbium-doped fiber lasers," *Photon. Res.*, vol. 4, no. 3, pp. 111–114, Jun. 2016.

[71] B. Guo *et al.*, "Observation of bright–dark soliton pair in a fiber laser with topological insulator," *IEEE Photon. Technol. Lett.*, vol. 27, no. 7, pp. 701–704, Jan. 2015.

[72] U. Teğin and B. Ortaç, "All-fiber all-normal dispersion femtosecond laser with a nonlinear multimodal interference-based saturable absorber," *Opt. Lett.*, vol. 43, no. 7, pp. 1611–1614, Apr. 2018.

[73] Z. Lv *et al.*, "Nonlinear multimodal interference for ytterbium-doped all-fiber mode-locking noise-like pulse generation," *Appl. Phys. Exp.*, vol. 12, no. 2, Jan. 2019, Art. no. 022004.

[74] Z. Dong, S. Li, P. Yao, C. Gu, and L. Xu, "Mode-locked fiber laser with offset splicing between two multimode fibers as a saturable absorber," *arxiv 1807.01037*, 2018.

[75] Z. Dong *et al.*, "Yb-doped all fiber picosecond laser based on grade-index multimode fiber with microcavity," *arxiv 1809.07174*, 2018.

[76] F. Zhao *et al.*, "Passively Q-switched all-fiber Yb-doped lasers based on nonlinear multimode interference," *J. Russian Laser Res.*, vol. 40, no. 1, pp. 87–93, 2019.

[77] P. Zhang, T. Wang, W. Ma, K. Dong, and H. Jiang, "Tunable multiwavelength Tm-doped fiber laser based on the multimode interference effect," *Appl. Opt.*, vol. 54, no. 15, pp. 4667–4671, May 2015.

[78] M. B. Shemirani, W. Mao, R. A. Panicker, and J. M. Kahn, "Principal modes in graded-index multimode fiber in presence of spatial- and polarization-mode coupling," *J. Lightw. Technol.*, vol. 27, no. 10, pp. 1248–1261, May 2009.

[79] D. A. Nolan, X. Chen, and M. J. Li, "Fibers with low polarization-mode dispersion," *J. Lightw. Technol.*, vol. 22, no. 4, pp. 1066–1077, Apr. 2004.

[80] T. Jannson, "Real-time Fourier transformation in dispersive optical fibers," *Opt. Lett.*, vol. 8, no. 4, pp. 232–234, Apr. 1983.

[81] K. Goda and B. Jalali, "Dispersive Fourier transformation for fast continuous single-shot measurements," *Nature Photon.*, vol. 7, pp. 102–112, 2013.

[82] H. J. Chen *et al.*, "Soliton booting dynamics in an ultrafast anomalous dispersion fiber laser," *IEEE Photon. J.*, vol. 10, no. 2, pp. 1–9, Apr. 2018, Art. no. 1501809.

[83] G. Wang, G. Chen, W. Li, C. Zeng, and H. Yang, "Decaying evolution dynamics of double-pulse mode-locking," *Photon. Res.*, vol. 6, no. 8, pp. 825–829, Aug. 2018.

[84] D. R. Solli, C. Ropers, P. Koonath, and B. Jalali, "Optical rogue waves," *Nature*, vol. 450, pp. 1054–1057, Jan. 2007.

[85] A. Zaviyalov, O. Egorov, R. Iliew, and F. Lederer, "Rogue waves in mode-locked fiber lasers," *Phys. Rev. A*, vol. 85, Jan. 2012, Art. no. 013828.

[86] J. M. Soto-Crespo, P. Grelu, and N. Akhmediev, "Dissipative rogue waves: Extreme pulses generated by passively mode-locked lasers," *Phys. Rev. E*, vol. 84, Jul. 2011, Art. no. 016604.

[87] M. Taki, A. Mussot, A. Kudlinski, E. Louvergneaux, M. Kolobov, and M. Douay, "Third-order dispersion for generating optical rogue solitons," *Phys. Lett. A*, vol. 374, no. 4, pp. 691–695, Jan. 2010.

[88] C. Kharif and E. Pelinovsky, "Physical mechanisms of the rogue wave phenomenon," *Eur. J. Mechanics B/Fluids*, vol. 22, no. 6, pp. 603–634, Nov.–Dec. 2003.

[89] A. Mussot, E. Louvergneaux, N. Akhmediev, F. Reynaud, L. Delage, and M. Taki, "Optical fiber systems are convectively unstable," *Phys. Rev. Lett.*, vol. 101, Sep. 2008, Art. no. 113904.

[90] L. Palmieri and A. Galtarossa, "Coupling effects among degenerate modes in multimode optical fibers," *IEEE Photon. J.*, vol. 6, no. 6, pp. 1–8, Dec. 2014.

[91] J. M. Fini and S. Ramachandran, "Natural bend-distortion immunity of higher-order-mode large-mode-area fibers," *Opt. Lett.*, vol. 32, no. 7, pp. 748–750, Apr. 2007.

[92] M. E. Fermann, A. Galvanauskas, and M. Hofer, "Ultrafast pulse sources based on multi-mode optical fibers," *Appl. Phys. B*, vol. 70, no. 1, pp. S13–S23, 2000.

[93] M. E. Fermann, L. M. Yang, M. L. Stock, and M. J. Andrejco, "Environmentally stable Kerr-type mode-locked erbium fiber laser producing 360-fs pulses," *Opt. Lett.*, vol. 19, no. 1, pp. 43–45, Jan. 1994.

[94] T. F. Carruthers, I. N. Duling, and M. L. Dennis, "Active–passive modelocking in a single-polarization erbium fiber laser," *Electron. Lett.*, vol. 30, no. 13, pp. 1051–1053, Jun. 1994.

[95] D. J. Jones, L. E. Nelson, H. A. Haus, and E. P. Ippen, "Diode-pumped environmental stable stretched-pulse fiber laser," *IEEE J. Sel. Topics Quantum Electron.*, vol. 3, no. 4, pp. 1076–1079, Aug. 1997.

[96] K. S. Chiang, "Intermodal dispersion in two-core optical fibers," *Opt. Lett.*, vol. 20, no. 9, pp. 997–999, May 1995.

[97] U. Levy and Y. Fainman, "Dispersion properties of inhomogeneous nanostructures," *J. Opt. Soc. Amer. A*, vol. 21, no. 5, pp. 881–889, May 2004.

[98] P. Walczak, S. Randoux, and P. Suret, "Optical rogue waves in integrable turbulence," *Phys. Rev. Lett.*, vol. 114, no. 14, Apr. 2015, Art. no. 143903.

[99] C. Zeng, Y. D. Cui, and J. Guo, "Observation of dual-wavelength solitons and bound states in a nanotube/microfiber mode-locking fiber laser," *Opt. Commun.*, vol. 347, pp. 44–49, Feb. 2015.

[100] M. Bernier *et al.*, "Bragg gratings photoinduced in ZBLAN fibers by femtosecond pulses at 800 nm," *Opt. Lett.*, vol. 32, no. 5, pp. 454–456, 2007.

[101] S. D. Jackson, "Towards high-power mid-infrared emission from a fibre laser," *Nature Photon.*, vol. 6, no. 7, pp. 423–431, Jun. 2012.

[102] X. Ma, C.-H. Liu, G. Chang, and A. Galvanauskas, "Angular-momentum coupled optical waves in chirally-coupled-core fibers," *Opt. Exp.*, vol. 19, no. 27, pp. 26515–26528, Dec. 2011.

[103] S. Ramachandran *et al.*, "Anomalous dispersion in a solid, silica-based fiber," *Opt Lett.*, vol. 31, no. 17, pp. 2532–2534, Sep. 2006.

[104] X. Xue *et al.*, "Mode-locked dark pulse Kerr combs in normal-dispersion microresonators," *Nature Photon.*, vol. 9, no. 9, pp. 594–600, Aug. 2015.

[105] Q.-F. Yang, X. Yi, K. Y. Yang, and K. Vahala, "Stokes solitons in optical microcavities," *Nature Phys.*, vol. 13, no. 1, pp. 53–57, Sep. 2017.

[106] P. Del'Haye, O. Arcizet, M. L. Gorodetsky, R. Holzwarth, and T. J. Kippenberg, "Frequency comb assisted diode laser spectroscopy for measurement of microcavity dispersion," *Nature Photon.*, vol. 3, pp. 528–532, Aug. 2009.

[107] L. Fang, Z. J. Wong, R. M. Ma, Y. Wang, and X. Zhang, "Single-mode laser by parit-time symmetry breaking," *Science*, vol. 346, no. 6212, pp. 972–975, Nov. 2014.

[108] H. Hodaei, M. Miri, M. Heinrich, D. N. Christodoulides, and M. Khajavikhan, "Parity-time-symmetric microring lasers," *Science*, vol. 346, no. 6212, pp. 975–978, Nov. 2014.